

Functional synergy of anti-mir221 and nanohydroxyapatite scaffold in bone tissue engineering of rat skull

Mahya Sadeghi¹ · Behnaz Bakhshandeh² · Mohammad Mehdi Dehghan³ ·
Mohammad Reza Mehrnia⁴ · Arash Khojasteh⁵

Received: 3 March 2016 / Accepted: 5 July 2016 / Published online: 12 July 2016
© Springer Science+Business Media New York 2016

Abstract An appropriate cell source, effective cell modification, and proper supportive matrices are the main bases of tissue engineering. The effectiveness of anti-mir221 or hydroxyapatite (HA) in improving the osteogenic differentiation of mesenchymal stem cells (MSCs) has been reported previously. Herein, simultaneous application of these osteogenic inducers was investigated *in vivo*. The Poly-caprolactone (PCL)/HA nanofibers were characterized using contact angle measurement, tensile test, Fourier transform infrared spectroscopy, and electron microscopy. Rat MSCs were isolated, characterized and transfected with anti-mir221. The rats were divided into 4 groups and an 8 mm defect were created in the mid-calvaria of each rat by trephine bur. Group 1 received (PCL)/HA nanofibers, group 2 received (PCL)/HA nanofibers plus autologous MSCs, group 3 received (PCL)/HA nanofibers plus MSCs transfected with anti-mir221, and group 4 rats were left

empty as an additional control group. Histomorphometric and radiomorphometric evaluation after 4 and 8 weeks revealed more new bone formation in the cell-treated groups compared to the scaffold alone group. There was evidence for a combination of increased osteoclasts and osteoblast vascular lake containing red blood cells in the anti-mir221 transfected group. New bone penetration into the scaffolds empirically demonstrated the capability of this combination for efficient osteointegration. Altogether, the co-application of HA and anti-mir221 transfected cells can enhance bone healing of the rat skull.

1 Introduction

A bone defect, caused by trauma or bone-related diseases, is considered a human health concern. Current therapeutic strategies mainly rely on tissue repair by transplantation of synthetic implants or natural grafts [1]. However, limitations of the current strategies have increased the interest in tissue engineering [2]. An appropriate cell source, effective cell modification, and proper supportive matrices are the main bases of tissue engineering. Determination of an effective combination of cell and matrix is a challenging issue for bone regeneration [3]. Mesenchymal stem cells (MSCs) are of intense interest in the field of regenerative medicine both for their differentiation potential and for the ability to serve as the functional part of a defined tissue [1].

Having unique features such as high porosity, large surface area, and an architecture mimicking ECM make nanofibers an interesting choice in tissue engineering [2]. Electrospinning is one of the best techniques for the controlled fabrication of nanofiber [3].

In addition to surface geometry and physical properties, chemical composition of the scaffold affects cell

Electronic supplementary material The online version of this article (doi:10.1007/s10856-016-5746-x) contains supplementary material, which is available to authorized users.

✉ Behnaz Bakhshandeh
b.bakhshandeh@ut.ac.ir

- ¹ Kish International Campus, University of Tehran, Tehran, Iran
- ² Department of Biotechnology, College of Science, University of Tehran, P.O. Box: 14155-6455, Tehran, Iran
- ³ Department of Clinical Sciences, Faculty of Veterinary Medicine, University of Tehran, Tehran, Iran
- ⁴ School of Chemical Engineering, University College of Engineering, University of Tehran, Tehran, Iran
- ⁵ Department of Tissue Engineering, School of Advanced Technologies in Medicine, Shahid Beheshti University of Medical Sciences, Tehran, Iran

attachment. Appropriate osteoconductivity, biodegradability, and direct bone-binding capability support the application of hydroxyapatite (HA) in bone reconstruction [1, 2]. HA helps scaffold integration into bone defects through increased protein adsorption and subsequent enhanced cell adhesion and proliferation [7, 8]. Nevertheless, the application of HA without additional ingredients is limited because of HA brittleness and poor mechanical stability [4].

Poly-caprolactone (PCL) is another biodegradable polymer commonly employed in tissue regeneration [10]. Migration of MSCs into the PCL scaffold results in rich extracellular matrix (ECM) production [5]. An *in vivo* study demonstrated mineralized ECM around a PCL scaffold in rats [6]. Another study reported enhanced osteogenic induction of PCL/HA/Poly-L-lactic acid scaffolds [13]. In addition, electrospinning is applied to overcome the possibility of HA embedding in the PCL fibers [2].

Recently, various regulatory molecular mechanisms of osteogenic differentiation have been uncovered. MicroRNAs (miRNAs) are short noncoding gene products that play important post-transcriptional regulatory roles in cell fate determination. They bind to messenger RNAs as master switches [14]. There is considerable evidence about the contribution of miRNAs in diverse processes such as bone development. The miRNA profile of stem cells undergoing osteogenic differentiation was reported previously [15]. In addition, the direct role of mir-221 down-regulation during osteogenic differentiation of MSCs was explained [7]. Based on previous findings, herein we investigated the co-application of anti-mir221 and nanohydroxyapatite in bone healing of the rat skull.

2 Materials and methods

2.1 Cell isolation and characterization

Isolation and expansion of rat MSCs were performed as described previously [17]. For cell characterization, specific CD markers (CD29, CD45, CD44, CD73, CD11b, and CD105) were analyzed by flow cytometry. MSCs (with an initial cell density of 10^4 cm^{-2}) were cultured in growth medium (high glucose DMEM with 10 % FBS and 1 % penicillin/streptomycin antibiotics, all from Gibco, UK) under a humidified atmosphere of 5 % CO_2 and 95 % air at 37 °C in 24-well tissue culture polystyrene plates.

2.2 miRNA transfection

MSCs were reverse transfected with anti-mir221 and Lipofectamine transfection reagent (all from Thermo Fisher Scientific) as described previously [7]. Briefly,

37.5 ng fluorescent miRNA was spotted in 100 μl culture medium without serum into a single well of a 24-well plate. After Lipofectamine supplementation, incubation for 5–10 min at room temperature allowed transfection complex formation. Following transfection complex formation, 8×10^4 cells in 250 μl of growth medium (without serum and antibiotics) were seeded into the well on top of the miRNA/Lipofectamine complexes and incubated under mild shaking at 37 °C and 5 % CO_2 for 6 h. Growth medium was then replaced by DMEM containing 10 % FBS and antibiotics, and incubated for 72 h. The cells were visualized by fluorescence microscopy (TE2000-S; Nikon), then washed and harvested for flow cytometry analysis.

2.3 Nanofiber fabrication and cell seeding

Nanofibers were fabricated by electrospinning. For PCL/HA scaffolds, suspension of nHA in chloroform (Merk) was prepared (20 wt % of polymer weight) and the PCL (in a solvent mixture of chloroform and DMF (8:2, v/v)) was dissolved in the HA suspension. Finally, the mixture was homogenized using a stirrer and ultrasonic homogenizer. Additional steps were performed as described previously [13]. PCL ($M_n = 80$) and nHA were purchased from Sigma-Aldrich. A low frequency plasma generator (44 kHz frequency) and a cylindrical quartz reactor (Diener Electronics, Germany) were used for oxygen plasma treatment. Prior to cell seeding, scaffolds were sterilized in 70 % ethanol and incubated in growth medium overnight.

2.4 Tensile strength analysis

The tensile strength of nanofibrous webs were measured using Galdabini testing equipment. The scaffolds were cut into $10 \times 50 \times 0.12 \text{ mm}^3$ specimens, and the tensile test was conducted at 20 mm/min crosshead speed at room temperature.

2.5 Fourier transform infrared (FTIR) spectroscopy

FTIR spectroscopy was performed to investigate the incorporation of HA into the electrospun PCL nanofibers with an Equinox 55 spectrometer (Bruker Optics, Germany).

2.6 Cell and fiber morphology evaluation

To assess the nanofiber morphology and cell attachment, the specimens were gold coated using a sputter coater and scanned using a scanning electron microscope (SEM, LEO 1455 VP, Cambridge, UK). For cell containing scaffolds, the specimens were fixed in 2.5 % glutaraldehyde for 1 h before gold coating. The mean diameter of fibers was

determined based on SEM images using image analysis software (ImageJ, NIH, USA).

2.7 Scaffold transplantation

Twelve adult male rats were maintained in standard conditions at 20 °C under 12/12 h periods of darkness/light. The experiments were performed in accordance with guidelines of the NIH on the care and use of animals for scientific purposes. Rats were anaesthetized using ketamine (20 mg/kg weight of mouse) and xylene (2 mg/kg weight of mouse) by intra-peritoneal injection. After hair cutting and disinfection, a midline incision was made from the nasofrontal area to the external occipital protuberance along the midsagittal suture. Subperiosteal dissection was performed bilaterally to expose the full extent of the calvaria. In each animal, one calvarial through-and-through osteotomy, 8.0 mm in diameter, was created in the dorsal portion of the parietal bone midsagittal suture using a surgical trephine bur (Messeinger, Dusseldorf, Germany) under irrigation with sterile normal saline. Finally, the surgery sites were stitched (supplementary Figure 2) and the bone healing was evaluated after 4 and 8 weeks.

The animals were randomly allocated into 4 groups of 3 animals each (Table 1). Group 1 (“scaffold” group) received PCL/HA nanofibers, group 2 (“cell + scaffold” group) received PCL/HA nanofibers plus autologous MSCs, group 3 (“transfected cell + scaffold” group) received PCL/HA nanofibers plus MSCs transfected with anti-mir221, and group 4 rats were left empty as a control group.

2.8 Histopathology and computed radiography

After 4 and 8 weeks, defect sites were harvested and fixed in 10 % neutral buffered formalin solution. Samples were washed and placed in sodium citrate/10 % formic acid solution for 45 days in order to complete decalcification. Each decalcified sample was dehydrated in alcohol. After embedding in paraffin, 8 µm sections were prepared from the center of defects and stained with Hematoxylin and Eosin (H&E). Histology slides were evaluated by light microscope. Digital images from computed radiography (CR) analysis were used to determine the bone density and the cortical thickness in the defect site of skull.

3 Results

3.1 Cell culture and characterization

Evaluation of cultured rat MSCs illustrated fibroblast-like and spindle-shaped morphology at low cell density. Also, the isolated rat MSCs were CD29+, CD45–, CD44+, CD73+, CD11b–, and CD105+ (Fig. 1).

3.2 Nanofiber characterization

FTIR spectra of PCL/HA composite nanofibers is shown in Fig. 2. The vibrations of PO₄³⁻ groups in HA resulted in characteristic peaks at 630 and 1016 cm⁻¹. The peak at 1723 cm⁻¹ in the spectrum could be due to a carbon–oxygen double bond in PCL.

A wetting angle of 136.35° was calculated before plasma radiation while the contact angle of a water droplet on the plasma-treated scaffold surface decreased to zero, which is the indication of water absorption. Contact angle measurement of a water droplet suggested the hydrophilicity correction of scaffold surface by plasma application. In addition, the result of tensile strength analysis showed no significant disturbance in the tensile properties of the plasma-treated scaffold (Fig. 2).

SEM micrographs of the scaffold showed properly aligned nano-scaled and beadless fibers fabricated under controlled conditions with homogeneously dispersed HA (Fig. 3a, supplementary Figure 1). The mean diameter of fibers was 650 ± 50 nm. Obviously, suitable cell attachment to the fibers was detected and no significant difference was detected among the groups regarding cell-fiber attachment (Fig. 3b, c).

3.3 In vivo evaluations

Bone healing and new bone formation at the site of injury were evaluated by CR and histopathology. One rat from group 2 and one rat from group 3 died before evaluation. More specimens are recommended for future studies.

3.4 Qualitative evaluation of CR images

At week 4, partial bone healing was only observed in the “transfected cell + scaffold” group (Fig. 4). At week 8, opacity evaluation by CR presented hard tissue formation in

Table 1 Description of the in vivo groups studied at 4 and 8 weeks

| Group number | Group name | Transplanted specimen |
|--------------|-----------------------------|--|
| Group 1 | Scaffold | Only scaffold |
| Group 2 | Cell + scaffold | Stem cell-seeded scaffold |
| Group 3 | Transfected cell + scaffold | Anti-mir221 transfected cell-seeded scaffold |
| Group 4 | Control | Defect with no transplantation |

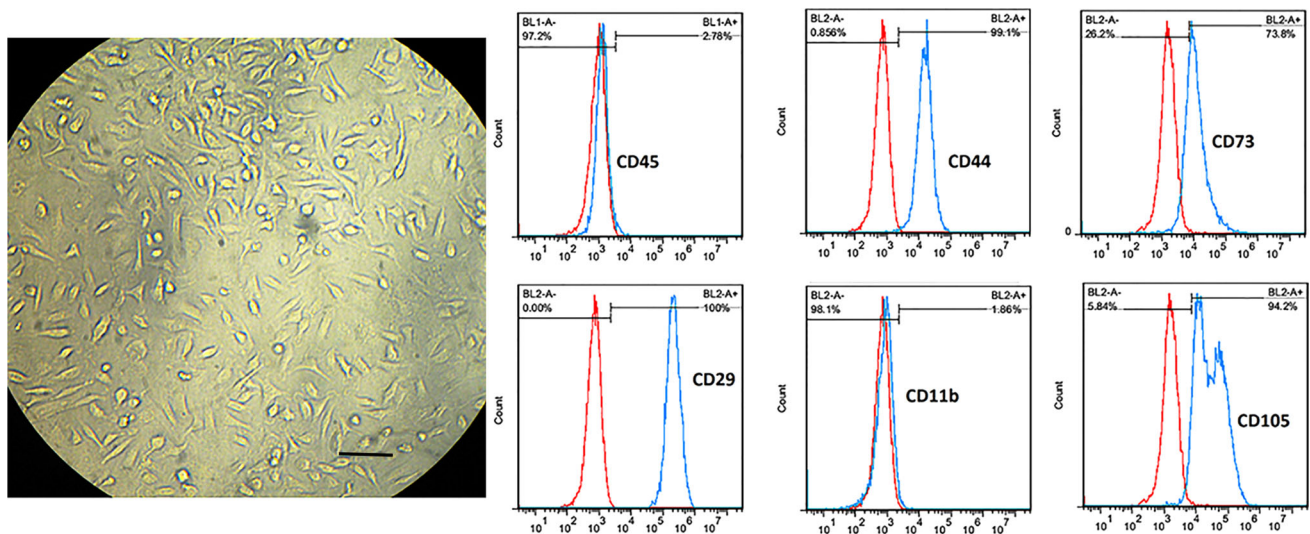
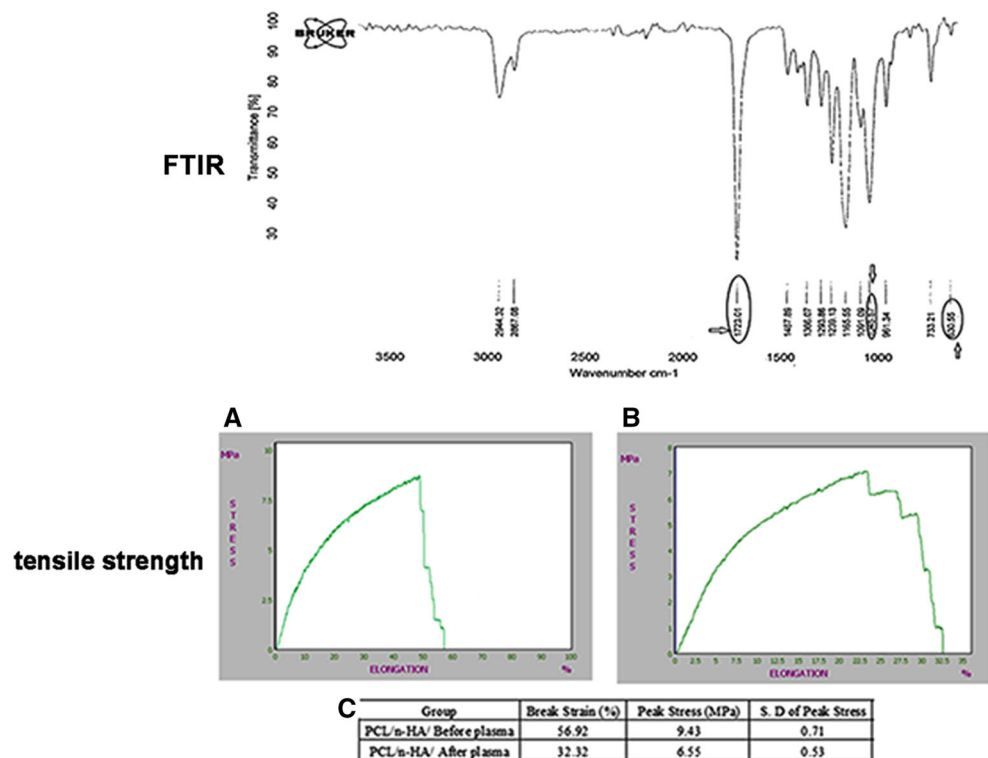


Fig. 1 Characterization of isolated rat MSCs. Phase-contrast microscopy of low-density cell culture MSCs showed spindle-like and square-shaped morphology. Scale bars 100 µm. Flow cytometry

analysis showed that the isolated rat MSCs were CD29+, CD45–, CD44+, CD73+, CD11b–, and CD105+

Fig. 2 Scaffold characterization, FTIR spectra of PCL/HA illustrated the incorporation of nHA into the scaffold. Stress–strain curves of aligned nanofibrous scaffolds along the fiber axis **a** before and **b** after plasma treatment showed no significant change in the tensile properties of the scaffold



both “cell + scaffold” group and “transfected cell + scaffold” group. No significant filling of the defect site was detected in the control group and the scaffold group.

3.5 Qualitative evaluation of histologic slides

Defect sites exhibited variable degrees of healing, ranging from limited bone formation in group 4 to nearly haphazard trabecular bone formation in group 2. Histological

evaluation indicated a mild chronic inflammatory response by infiltration of mononuclear inflammatory cells in the defect area in all groups. In addition, a narrow bridge of connective tissue (collagen fibers) was formed in the defect area.

At week 4 the remnant of PCL scaffold was noticeable in all groups while at week 8, PCL/HA underwent degradation and could hardly be detected in the scaffold-containing group (Fig. 5).

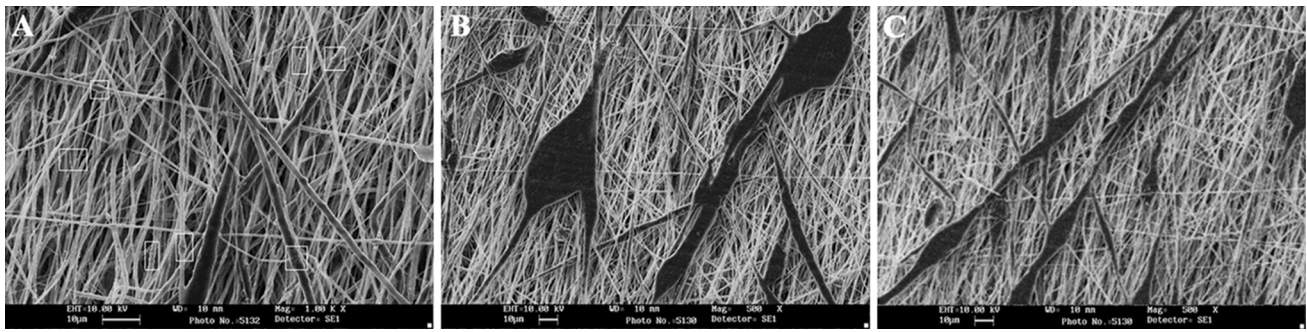


Fig. 3 SEM micrographs demonstrated bead-free and properly oriented structure of fabricated scaffolds (a, $\times 1000$), and the incorporation of nHA particles into the PCL fibers and consequent rough surface is obvious. Cell attachment evaluation:

“Cell + Scaffold” group (b, $\times 500$) and “Transfected cell + Scaffold” group (c, $\times 500$). As shown, no significant difference was found regarding the cell attachment in cell containing groups

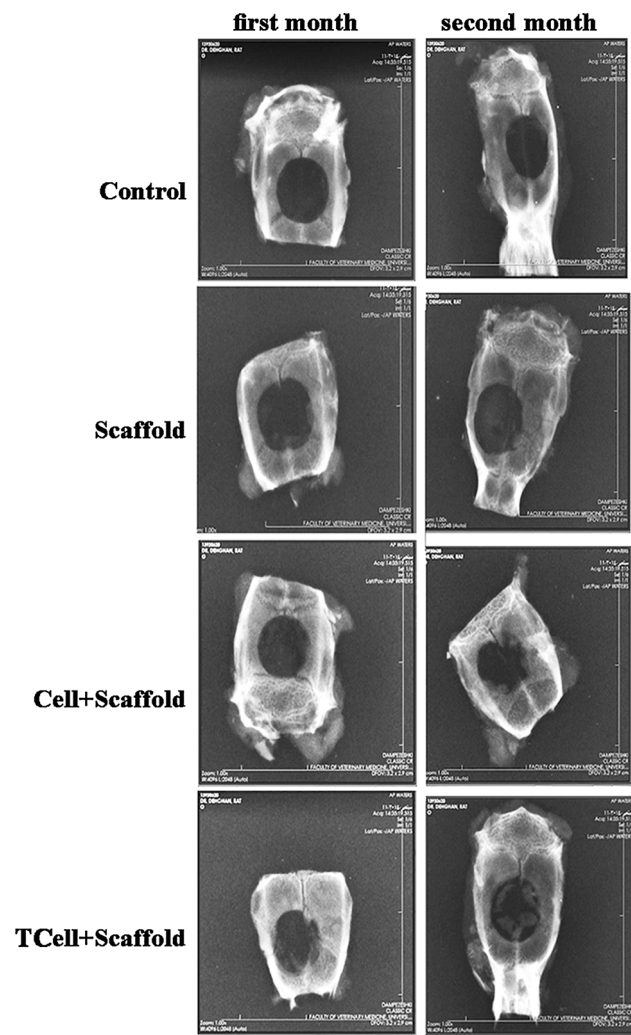


Fig. 4 Computed radiography images of rat calvaria after first and second month evaluations in four groups (control: untreated damaged site, scaffold: pure PCL/nHA scaffold, cell + Scaffold: cell-seeded scaffold, and T cell + Scaffold: anti-mir221 transfected cell-seeded scaffold)

New Bone formation from the original border of the calvaria bone was evident in all groups from peripheral to central direction that was remarkably more in cell treated groups (Fig. 6). In 2 specimens from the cell + scaffold group, the defects showed half-length bone healing. At the periphery, lamellar bone could be detected near the original recipient site bone (Fig. 7). Trabecular bone formation was evident within the scaffold at the central part of the defect far away from the original border. Osteoblast-like cells exhibiting a dense arrangement adjacent to newly formed bone suggests continuous bone formation through the center of the defect. However, less bone formation activity was evident at the center of the defects in cell free groups (groups 1 and 4). There was no evidence of fatty marrow or cartilage formation. The newly formed bone consisted trabecular bone. Lamellar bone formation could not be detected in the central part of defects in any of the groups after 8 weeks of healing. In the cell + scaffold group, a more obvious finding of osteoblast-like cells and direct bone to biomaterial contact was observed (Fig. 8).

In group 3 the co-application of anti-mir221 transfected cells and PCL/HA scaffold resulted in trabecular bone with less cellularity in the center of the defect. Qualitative histological evaluation demonstrated some spherical buds scattered throughout the defects in this group (Fig. 9). The presence of multi nucleated cells, vascular lake and cuboid osteoblast like cells, resembles these bud-to-bone metabolic units. The rate of lamellar to trabecular bone was found to be more in the transfected cell + scaffold group.

4 Discussion

Discovering the most effective combination of proper cell and matrix is an important aim in tissue engineering. Recently, a few in vivo studies have investigated certain

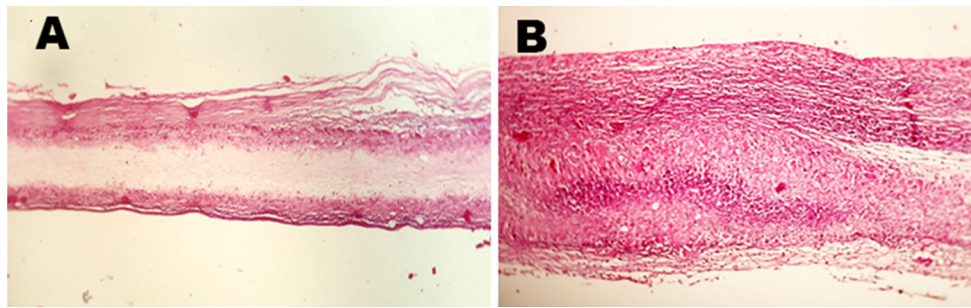


Fig. 5 (a) PCL/HA Scaffold at 4 weeks and (b) degradation of the scaffold at 8 weeks (H&E*10)

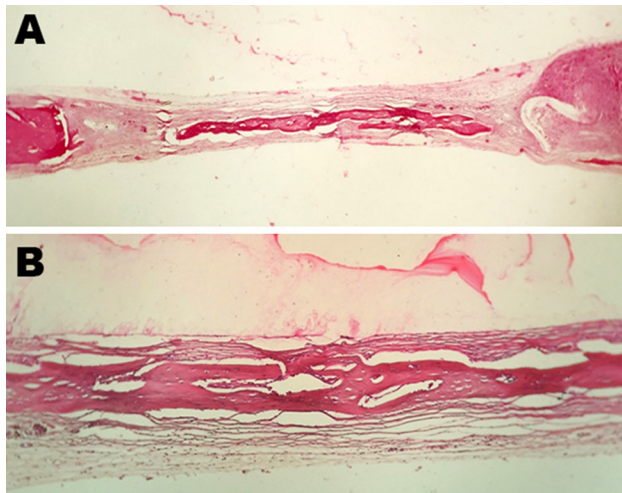


Fig. 6 Trabecular Bone formation within the defects. a H&E*10 b H&E*40

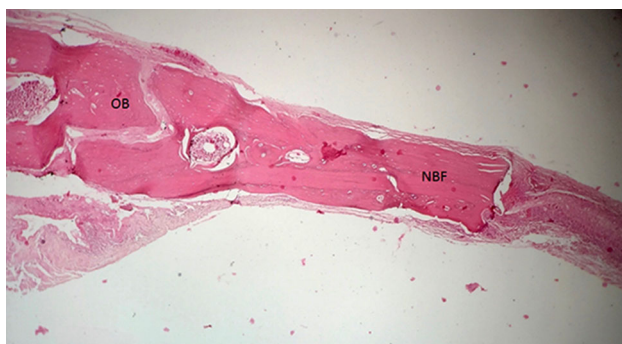


Fig. 7 Lamellar bone formation could be detected in the peripheral part of the defect in the cell treated group (H&E*20). *OB* original bone, *NBF* new bone formation

cell modifying factors such as mir-26a [8] or mir-31 [19] in bone healing. Regarding the noticeable results of this strategy in effective healing, more investigation would be valuable.

Our team has demonstrated the inductive effect of mir-221 downregulation in osteogenic differentiation of MSCs

[7]. Based on bioinformatic analysis, the sequences of mature mir-221 in both human and rat are identical (supplementary Doc. 1). High conservation of the mir-221 sequence suggests the important function of this miRNA during animal evolution. According to our previous studies, transfection efficiency of miRNA into MSCs was about 86 % [9]. Therefore, we considered studying the role of anti-mir221 transfected MSCs in bone healing of rat skull.

Enhanced osteogenic differentiation of stem cells by PCL/HA scaffold in vitro was explained previously [10]. Several in vivo studies attempted to enhance bone healing with implants containing cells and HA. For instance, subcutaneous implantation of HA/tricalcium phosphate (TCP) composite blocks and rat MSCs resulted in the establishment of endochondral bone tissue [21]. Another study proposed bone-mimetic electrospun matrices composed of PCL/collagen/HA and MSCs for bone regeneration [22]. Subcutaneous implantation of PCL/HA and ionically modified carbon nanotube scaffolds in rat showed similar tissue reaction to those with PCL/HA scaffolds [23]. Rat bone marrow mesenchymal stem cells (BM-MSCs) delivered by beta TCP have demonstrated more bone formation in a 5 mm through and through calvaria defect than platelet rich plasma [11]. When delivered with HA/TCP or nano-HA MSCs these cells showed promising results compared to the cell free group [12, 13]. Therefore, we utilized a PCL/HA scaffold in order to transplant anti-mir221 transfected MSCs into rat skull defects. In order to prevent possible rejection and inflammation, rat MSCs were used in rat models. These cells were isolated, expanded, and characterized (Fig. 1).

Adherent cells convert signals from sensing matrix topography into morphological alterations. Electrospun nanofibers have gained an up-trust because of the ability to biomimick the ECM structure [3]. Relatively small pore size between the electrospun fibers leading to limited cell infiltration could be corrected by aligned fabrication [14]. Aligned electrospun PCL/HA nanofibrous scaffolds were successfully fabricated and characterized. Surface wettability is an important property of biomaterials affecting cell

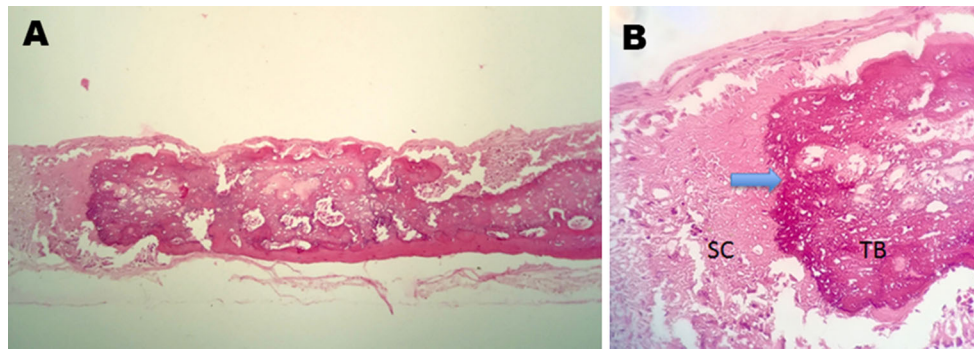


Fig. 8 **a** Trabecular bone formation within the scaffold in the cell treated group (H&E*10); **b** Direct contact of new bone was evident in contact with PCL/HA scaffold. *Arrow* shows the Contact line. *TB* trabecular bone, *SC* scaffold

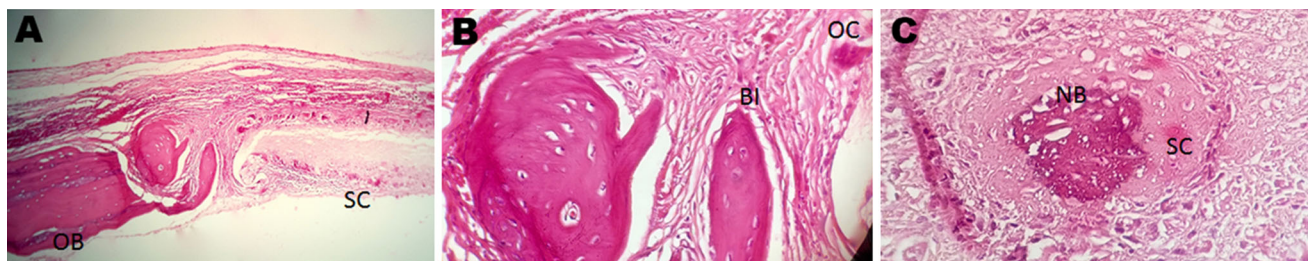


Fig. 9 **a** Island of new lamellar bone formation between a remnant of scaffold and original bone (H&E*10); **b** Direct lamellar bone formation (H&E*40); **c** Emerging new bone within the scaffold (H&E*40). *OB* Original bone, *SC* scaffold, *BI* bone Island, *OC* Osteoclast like cells

attachment and proliferation [15]. Due to the hydrophobicity of PCL fibers, oxygen plasma treatment was applied. The water contact angle of plasma treated PCL/nHA nanofibers decreased to 0° , which demonstrated hydrophilicity of the plasma-treated scaffold. Analyses of FTIR spectra of PCL/HA composite nanofibers indicated effective incorporation of HA into the PCL nanofibers (Fig. 2), and the location of HA on the surface of the fibers led to a rough surface morphology that is ideal for cell attachment (Fig. 3). SEM micrographs presented uniform and aligned HA-incorporated nanofibers with interconnected pores, which could facilitate nutrient transport and cell in-growth (Fig. 3a, supplementary Figure 1). Suitable cell attachment to the nanofibers supported the biocompatibility of the scaffold, and no significant alteration was observed in cell attachment after anti-mir 221 transfection (Fig. 3b, c).

For in vivo evaluations, scaffolds (with or without the cells) were transplanted into the skulls in four groups (Table 1, supplementary Figure 2). After 4 and 8 weeks, bone healing and new bone formation were evaluated by computed radiology (CR) and histopathology. Opacification of the defects by CR demonstrated partial bone healing in both the “cell + scaffold” group and “transfected cell + scaffold” groups at week 8 (Fig. 4). Overall, no significant healing was observed in control group and scaffold group.

Results of histopathological analysis showed replacement of scaffolds by connective tissue after two months, which confirmed the in vivo biodegradability of PCL/HA scaffolds (Fig. 5).

The cell treated group showed a profound inflammatory reaction whilst transfected cell + scaffold group had less. High cellular trabecular bone, which was evident in the central part of cell treated groups, also has been replaced by direct emerging of lamellar bone from the scaffold throughout the calvaria defect in the anti-mir221 transfected cell + scaffold group. Both the MSCs and anti-mir221 transfected cell groups showed a higher amount of bone formation than the control and scaffold only groups.

Proper bone regeneration after 2 months using in vivo PCL/biphasic calcium phosphate scaffold transplantation was reported previously [16]. The degree of trabecular bone formation measured with light microscopy showed a significant difference between samples receiving the cells (groups 2 and 3) and the other groups (groups 1 and 4). Therefore, adding MSCs caused a slight tendency toward higher levels of trabecular bone formation. Taking these results into account, application of stem cells for transplantation could improve bone healing and the efficiency of tissue regeneration.

“Bone multicellular units” or “bone metabolic units” (BMUs) are functional groups of cells that progress through bone remodeling, removing old bone and replacing

it with new bone [17, 18]. BMUs are responsible for remodeling approximately 10 % of the skeleton, and are composed of different cell types such as osteoblasts, osteoclasts, and uncharacterized mononuclear cells [19]. The presence of multinucleated cells, vascular lake and cuboid osteoblast like cells, resembles the bud to bone metabolic units in the transfected cell + scaffold group. Formation of these units could be seen as a remarkable sign of effective healing. Such favorable results could be related to anti-mir221 transfected MSCs that might act as osteoblast progenitors [7]. Utilization of the other kinds of staining to detect different kinds of cells is recommended for future study.

Altogether, using a composite scaffold for cell delivery and transfection of cells with anti-mir221 improved new bone regeneration in a rat critical sized defect. New bone penetration into the scaffolds empirically demonstrated the capability of using this combination for efficient osteointegration. Altogether, this combination could introduce a new therapeutic strategy for orthopedic defects.

Acknowledgments Iran national science foundation financially supported this work.

Compliance with ethical standards

Conflict of interest The authors have no conflicts of interest.

References

- Barrilleaux B, Phinney DG, Prockop DJ, O'Connor KC. Review: ex vivo engineering of living tissues with adult stem cells. *Tissue Eng.* 2006;12(11):3007–19.
- Gupta D, Venugopal J, Mitra S, Giri Dev VR, Ramakrishna S. Nanostructured biocomposite substrates by electrospinning and electrospinning for the mineralization of osteoblasts. *Biomaterials.* 2009;30(11):2085–94.
- Murugan R, Ramakrishna S. Design strategies of tissue engineering scaffolds with controlled fiber orientation. *Tissue Eng.* 2007;13(8):1845–66.
- Wang M. Developing bioactive composite materials for tissue replacement. *Biomaterials.* 2003;24(13):2133–51.
- Yoshimoto H, Shin YM, Terai H, Vacanti JP. A biodegradable nanofiber scaffold by electrospinning and its potential for bone tissue engineering. *Biomaterials.* 2003;24(12):2077–82.
- Shin M, Yoshimoto H, Vacanti JP. In vivo bone tissue engineering using mesenchymal stem cells on a novel electrospun nanofibrous scaffold. *Tissue Eng.* 2004;10(1–2):33–41.
- Bakhshandeh B, Hafizi M, Ghaemi N, Soleimani M. Down-regulation of miRNA-221 triggers osteogenic differentiation in human stem cells. *Biotechnol Lett.* 2012;34(8):1579–87.
- Zhang X, Li Y, Chen YE, Chen J, Ma PX. Cell-free 3D scaffold with two-stage delivery of miRNA-26a to regenerate critical-sized bone defects. *Nature communications.* 2016;7:10376.
- Bakhshandeh B, Soleimani M, Hafizi M, Ghaemi N. A comparative study on nonviral genetic modifications in cord blood and bone marrow mesenchymal stem cells. *Cytotechnology.* 2012;64(5):523–40.
- Bakhshandeh B, Soleimani M, Ghaemi N, Shabani I. Effective combination of aligned nanocomposite nanofibers and human unrestricted somatic stem cells for bone tissue engineering. *Acta Pharmacol Sin.* 2011;32(5):626–36.
- Khojasteh A, Eslaminejad MB, Nazarian H. Mesenchymal stem cells enhance bone regeneration in rat calvarial critical size defects more than platelet-rich plasma. *Oral Surg Oral Med Oral Pathol Oral Radiol Endod.* 2008;106(3):356–62 **discussion 63.**
- Jafarian M, Eslaminejad MB, Khojasteh A, Mashhadi Abbas F, Dehghan MM, Hassanizadeh R, et al. Marrow-derived mesenchymal stem cells-directed bone regeneration in the dog mandible: a comparison between biphasic calcium phosphate and natural bone mineral. *Oral Surg Oral Med Oral Pathol Oral Radiol Endod.* 2008;105(5):e14–24.
- Behnia H, Khojasteh A, Kiani MT, Khoshzaban A, Mashhadi Abbas F, Bashtar M, et al. Bone regeneration with a combination of nanocrystalline hydroxyapatite silica gel, platelet-rich growth factor, and mesenchymal stem cells: a histologic study in rabbit calvaria. *Oral Surg Oral Med Oral Pathol Oral Radiol.* 2013;115(2):e7–15.
- Kurpinski KT, Stephenson JT, Janairo RR, Lee H, Li S. The effect of fiber alignment and heparin coating on cell infiltration into nanofibrous PLLA scaffolds. *Biomaterials.* 2010;31(13):3536–42.
- Yang J, Bei J, Wang S. Enhanced cell affinity of poly (D, L-lactide) by combining plasma treatment with collagen anchorage. *Biomaterials.* 2002;23(12):2607–14.
- Padalhin AR, ThuyBaLinh N, KiMin Y, Lee BT. Evaluation of the cytocompatibility hemocompatibility in vivo bone tissue regenerating capability of different PCL blends. *J Biomater Sci Polym Ed.* 2014;25(5):487–503.
- Parfitt AM, Drezner MK, Glorieux FH, Kanis JA, Malluche H, Meunier PJ, et al. Bone histomorphometry: standardization of nomenclature, symbols, and units. report of the ASBMR Histomorphometry Nomenclature Committee. *J Bone Miner Res.* 1987;2(6):595–610.
- Pogoda P, Priemel M, Rueger JM, Amling M. Bone remodeling: new aspects of a key process that controls skeletal maintenance and repair. *Osteoporos int.* 2005;16(Suppl 2):S18–24.
- Robling AG, Castillo AB, Turner CH. Biomechanical and molecular regulation of bone remodeling. *Annu Rev Biomed Eng.* 2006;8:455–98.